AIAA 2010-3714

Multiple Pure Tone Noise Prediction for Acoustically Treated Aircraft Engines

Umesh Paliath*, Fei Han†, Chingwei M. Shieh‡, and Anupam Sharma§
Energy and Propulsion Technologies,
General Electric Global Research Center, One Research Circle, Niskayuna, NY, 12309, USA

A multiple pure tone noise prediction approach for acoustically treated aero-engine inlets is described. It consists of three steps that account for noise source generation, nonlinear acoustic propagation with lined walls inside the nacelle, and linear acoustic propagation outside the engine. The predictions are compared with static test measurements for a typical high bypass ratio engine at inlet nacelle unsteady pressure transducer, near-field microphone array, and far-field microphone array locations.

I. Introduction

Multiple pure tone (MPT) noise, also referred to as "buzzsaw" noise, is characterized as multiple tones at frequencies that are harmonics of the engine shaft frequency. It is generated when the relative tip Mach number of the fan blade becomes supersonic and the rotor-locked pressure field can propagate out through the inlet. For a rotor with identical blades, identically repeating (in time) pressure pattern would be observed, which would result in noise at the fundamental and higher harmonics of the rotor blade passing frequency. However, due to minor blade-to-blade manufacturing variations, the pressure (shock) pattern is irregular in the circumferential direction and sub-harmonics of the rotor blade passing frequency are generated. Due to the non-linear propagation of these large-amplitude pressure waves, these irregularities grow as the disturbances propagate upstream (in the inlet duct) and more and more energy from the blade fundamental harmonic gets transferred into the sub-harmonics. The variation in blade-to-blade stagger angles is known[1] to be the dominant feature that determines the strength of the MPTs generated. Stagger angle differences as small as 0.1 degrees can result in substantial MPT noise generation.

Han *et al.*[2] presented an integrated numerical procedure to predict the generation, in-duct propagation, and radiation of MPT noise for hard-walled nacelles. Computational fluid dynamics (CFD) simulations were performed to generate the pressure field upstream of the fan blades. A linear superposition method[1,2] was used to reconstruct the pressure field for arbitrary fan blade stagger angle configurations. A one-dimensional (1-D) non-linear propagation model developed by McAlpine and Fisher[3,4] was used to investigate the propagation of MPT to the nacelle lip. Linear acoustic propagation from the nacelle lips to far field location was modeled using a commercial turbo-machinery acoustic software, ACTRAN/TM. The entire analysis process was applied to predict the MPT noise of a typical high bypass ratio engine with hardwall nacelle.

In the current paper, the same MPT prediction process is applied to the same engine with acoustic lining in the inlet duct. Liner acoustic attenuation is modeled using the assumption of a uniform mean flow in the nacelle, as well as the assumption of a sheared flow with thin boundary layers. The biggest approximation, as will be noted later, is the assumption that the presence of liners does not scatter the acoustic energy into different radial modes. Also, the behavior of the liner is assumed to remain unchanged by the nonlinearity of the acoustic waves. Sound pressure levels are compared between static engine test data and predictions for in-duct Kulite measurements, and near- and far-field microphone array measurements.

*Mechanical Engineer, Computational Heat Transfer and Aero Acoustics Lab, K1 2C-15A, AIAA Member
†Mechanical Engineer, Combustion Lab, ES-513, AIAA Member
‡Fluid Mechanics Engineer, Computational Heat Transfer and Aero Acoustics Lab, K1 2C-37A, AIAA Member
§Mechanical Engineer, Computational Heat Transfer and Aero Acoustics Lab, K1 2C-25A, AIAA Member

II. Prediction Process

A brief summary of the MPT prediction process (described in detail in Ref.[2]) is provided here for completeness -

1. A couple of part annulus RANS (Reynolds Averaged Navier-Stokes) solutions are combined using linear superposition to estimate the irregular pressure field right upstream of the fan. The irregularity in the pressure field can be attributed primarily to blade-to-blade variations in blade stagger angle. These are assumed to be known.

   The linear superposition model was validated against a full-annulus 2-D simulation and the results from Ref.[2] are plotted in Figs. 1 and 2. The importance of phase correction (matching) during the linear superposition was emphasized by comparing the results obtained with and without phase matching in Fig. 2.

(a) Started (b) Unstarted

Figure 1. A 2-D full annulus simulation with stagger variation in blades to predict MPT generation. (a) started fan, and (b) unstarted fan.

2. The one-dimensional nonlinear Burgers equation is then solved in the frequency domain to propagate the pressure field (shocks) inside the duct as described by McAlpine and Fisher.[3,4] The primary assumption here is that for each circumferential mode, m, only the lowest radial order mode $[m, 0]$ contains all the acoustic energy, which is never scattered into higher order radial modes. In frequency domain the nonlinear propagation equation can be written as

$$\frac{\mathrm{d}C_m}{\mathrm{d}T} = \frac{im\pi}{B}\left(\sum_{l=1}^{m-1} C_{m-l}C_l + 2\sum_{l=m+1}^{\infty} C_l\tilde{C}_{l-m}\right) - \epsilon\frac{m^2}{B^2}C_m - \sigma_m C_m, \tag{1}$$

   where, m is the circumferential order of an acoustic mode, C_m is the complex amplitude of the m^{th} mode, i.e., the amplitude of the m^{th} harmonic tone, T is the non-dimensional time, B is the number of blades, ϵ is a dissipation factor to account for the energy lost by nonlinear dissipation in modes that are ignored during the numerical calculation, and σ_m is a damping factor to be used to model the attenuation effect of the acoustic liner. σ_m was set to zero for all harwall computations in Ref.[2] The first term on the right hand side of Eq. 1 represents the nonlinear interaction among different tones or acoustic modes. The second term is used to account for dissipation at higher frequencies in numerical implementation of the equation where only a finite set of modes can be considered.

   Validation of the nonlinear propagation model against 2-D full-annulus CFD solution was also reported[2] and is repeated in Fig. 3

3. After shocks propagate through the liner and reach the end of the liner, the amplitudes are damped low enough that propagation onward can be considered a linear process. The linear propagation and

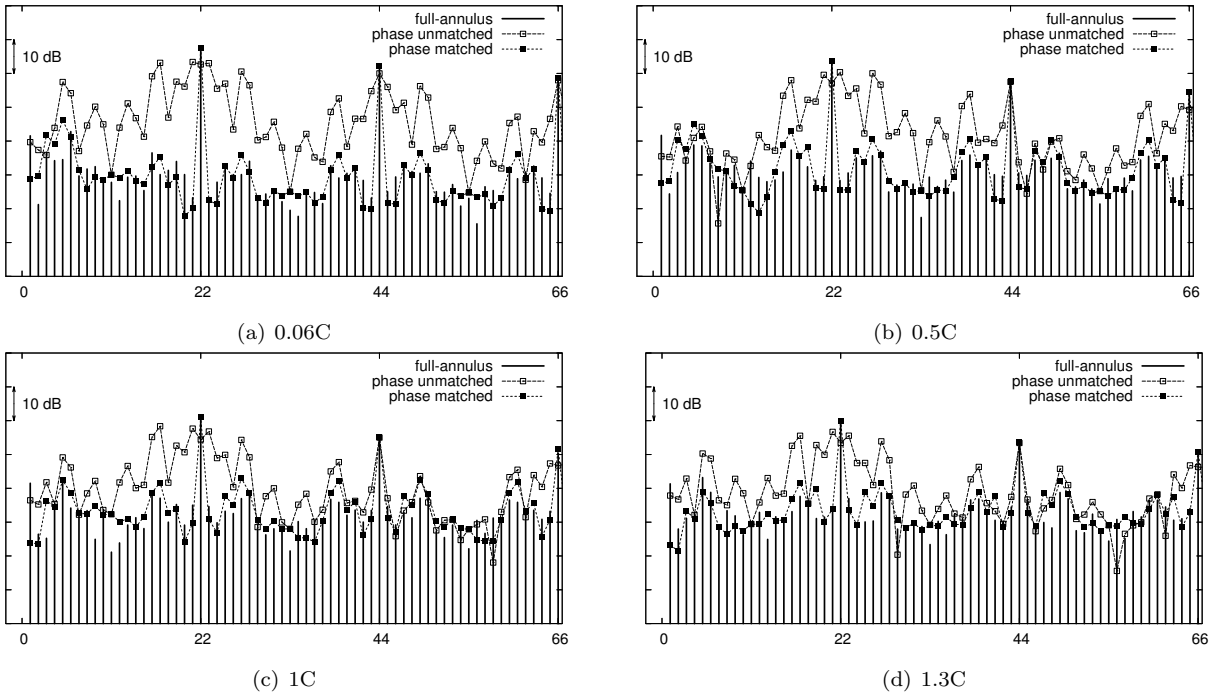

(a) 0.06C

(b) 0.5C

(c) 1C

(d) 1.3C

Figure 2. Validation of the linear superposition algorithm "superpose" against 2-D full-annulus simulations. Comparison presented for both phase-matched and phase un-matched results. Distance from the leading edge of the fan: (a) 0.06C, (b) 0.5C, (c) 1C, and (d) 1.3C , where C is the tip chord.

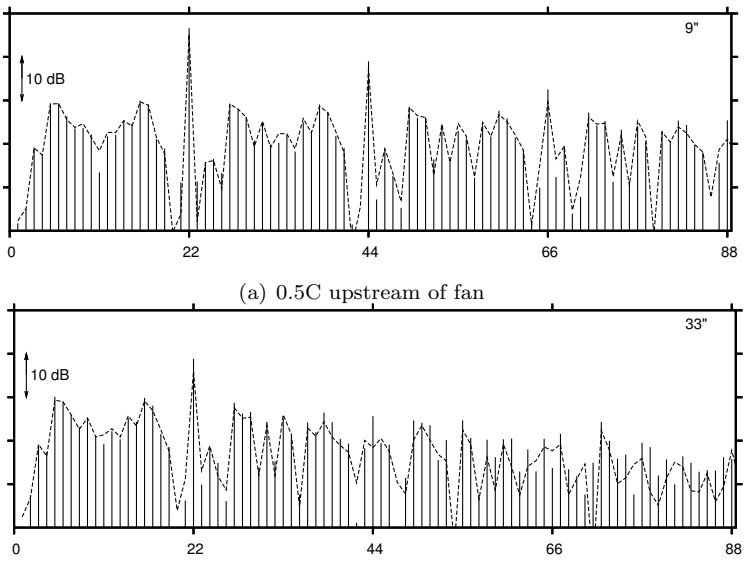

(a) 0.5C upstream of fan

(b) 1.3C upstream of fan

Figure 3. Comparison of spectra predicted by the nonlinear model against those obtained from direct Fourier transform from CFD solution at two axial distances upstream of the fan (a) 0.5C and (b) 1.3C.

radiation into far field outside of nacelle is calculated using ACTRAN/TM. The acoustic velocity potential is solved with a conventional finite element method (FEM) inside the computational domain and an infinite element method in the unbounded far-field domain.[5]

III. Acoustic Attenuation Modeling

A. Uniform Flow Approach

The attenuation factor, σ_m is obtained by solving the classical eigen-value problem of acoustic mode propagation in cylindrical ducts. McAlpine and Fisher[3] assumed a uniform mean flow in the duct, in which case the acoustic propagation equation can be written as[6] -

$$\frac{\mathrm{d}^2P}{\mathrm{d}r^2} + \frac{1}{r}\frac{\mathrm{d}P}{\mathrm{d}r} + \left\{\eta^2\left[\left(1 - M\frac{k_x}{\eta}\right)^2 - \left(\frac{k_x}{\eta}\right)^2\right] - \frac{m^2}{r^2}\right\}P = 0 \tag{2}$$

where, P is the acoustic pressure, r is the radius normalized by the casing radius, η is the non-dimensional frequency, M is the Mach number, k_x is the non-dimensional axial acoustic wavenumber. For soft wall ducts, the acoustic boundary condition at r=1 is

$$\frac{\mathrm{d}P}{\mathrm{d}r}\Big|_{r=1} = -i\eta A\left(1 - M\frac{k_x}{\eta}\right)^2 P, \tag{3}$$

where A is the acoustic admittance of the liner normalized by $\rho_0 c$. In the cylindrical duct case, the radial acoustic pressure variation is represented by the Bessel functions of the first kind, denoted here by J_m. The eigen-value equation then becomes

$$\kappa\frac{J_m'(\kappa)}{J_m(\kappa)} = -i\eta A\left(1 - M\frac{k_x}{\eta}\right)^2, \tag{4}$$

with

$$\frac{k_x}{\eta} = \frac{1}{1-M^2}\left[-M \pm \sqrt{1 - (1-M^2)\left(\frac{\kappa}{\eta}\right)^2}\right], \tag{5}$$

where, κ is the non-dimensional radial wavenumber. Equations 4 and 5 are combined to solve for the axial wavenumber, k_x. The imaginary part of k_x, which represents the damping due to the acoustic liner, is simply σ_m in Eq. 1

B. Effect of Boundary Layer on Liner Attenuation

The assumption of uniform mean flow was used in deriving Eqs. 2 and 3. In reality, due to the no-slip boundary condition at the nacelle wall, the mean flow varies in the radial direction, with $M = 0$ at the wall. Assuming the sheared velocity profile is known, the acoustic propagation equation for a cylindrical duct can be written as

$$\frac{\mathrm{d}^2P}{\mathrm{d}r^2} + \left[\frac{1}{r} + \frac{2k_x}{\eta - Mk_x}\frac{\mathrm{d}M}{\mathrm{d}r}\right]\frac{\mathrm{d}P}{\mathrm{d}r} + \left\{\eta^2\left[\left(1 - M\frac{k_x}{\eta}\right)^2 - \left(\frac{k_x}{\eta}\right)^2\right] - \frac{m^2}{r^2}\right\}P = 0 \tag{6}$$

with the boundary condition at the wall specified as

$$\frac{\mathrm{d}P}{\mathrm{d}r}\Big|_{r=1} = -i\eta AP. \tag{7}$$

Ideally, the attenuation factor σ_m in the nonlinear code should be obtained by solving the eigen-value problem given by Eqs. 6 and 7. However, these are difficult to solve for a mean flow with boundary layers.

For cases where the boundary layer is thin compared to the duct radius, Eversman[7] produced an asymptotic approach that still uses Eq. 6 for axial propagation and an equivalent boundary condition that should be enforced at the edge of the boundary layer. This equivalent boundary condition is

$$\frac{\mathrm{d}P}{\mathrm{d}r}\Big|_{r=1} = -\frac{(1 - M_0K)^2\left\{i\eta A + \delta\left[\beta\int_0^1 \mathrm{d}\xi/(1 - M_0K\phi)^2 - \alpha\right]\right\}}{1 + i\delta\eta A\int_0^1(1 - M_0K\phi)^2\mathrm{d}\xi}P, \tag{8}$$

where, δ is the boundary layer thickness normalized by the duct radius, M_0 is the core mean flow Mach number, $K = k_x/\eta$, $\alpha = \eta^2 - i\eta A$, $\beta = m^2 + \eta^2 K^2$. The velocity profile in the boundary layer is given by

$$M(\xi) = M_0\phi(\xi), \quad 0 \le \xi \le 1, \tag{9}$$

where $\xi = 1$ corresponds to the outer edge of the boundary layer. Clearly when $\delta = 0$, Eq. 8 is reduced to Eq. 3, the boundary condition for the case of uniform mean flow. Myers and Chuang[8] improved upon the asymptotic approach and obtained

$$\left.\frac{\mathrm{d}P}{\mathrm{d}r}\right|_{r=1} = -i\eta A(1-M_0K)^2P - \delta\left[\kappa^2 - m^2 + \kappa^2\frac{J_m'^2(\kappa)}{J_m^2(\kappa)}\left(1 - \int_0^1 \frac{h(\xi)}{h_0}\mathrm{d}\xi\right) - h_0\int_0^1 \frac{h(\xi) - \xi^2 - m^2}{h(\xi)}\mathrm{d}\xi\right] P, \tag{10}$$

where $h(\xi) = (\eta - k_x M_0\phi(\xi))^2$. Note that when $\delta = 0$, Eq. 10 also reduces to Eq. 3 of the uniform mean flow case. Myers and Chuang compared this approach with the one by Eversman and showed that their approach improved the accuracy for thicker boundary layers. Equations 2 and 10 are then used to solve the eigenvalues to obtain the liner attenuation factor, σ_m.

C. Results

The Myers-Chuang approach described in Section B is used to investigate the boundary layer effect on the liner attenuation. The boundary layer is assumed to have a linear profile (see 4 (a)). Figure 4 (b) plots the attenuation factor, $Im(k_x)$ as a function of boundary layer thickness for four circumferential mode orders.

For the mode of circumferential order 3 (EO=3), the boundary layer thickness does not seem to have much effect on the axial attenuation of the mode. As the mode order is increased, the boundary layer effect becomes more significant. This can be explained by comparing the corresponding cylindrical hardwall duct mode shapes for the two modes in Fig. 4 (c) obtained using a uniform meanflow assumption. As the circumferential order of the mode increases, its mode shape and hence acoustic energy gets weighted more and more towards the casing. Hence the impact of the boundary layer on liner attenuation increases with increasing mode order.

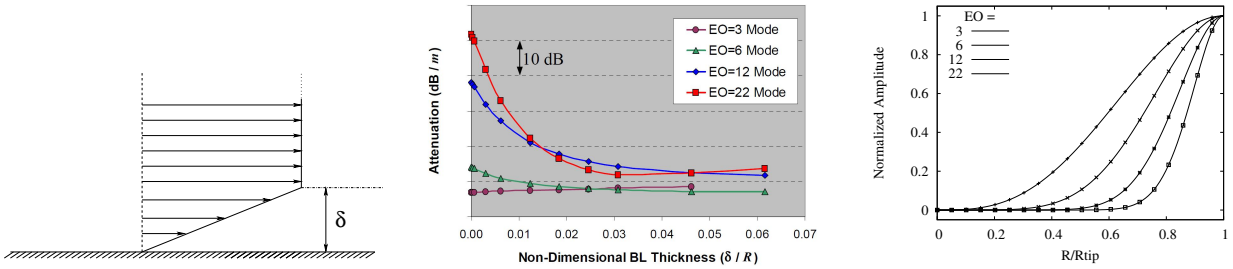

(a) Assumed boundary layer profile (b) Attenuation effect (c) Mode shape

Figure 4. Impact of boundary layer thickness, δ on the attenuation factor: (a) linear boundary layer profile assumed, (b) attenuation per unit length, and (c) duct mode (first radial order) shapes for engine orders 3, 6, 12, and 22.

IV. MPT Prediction and Comparison with Data

The MPT prediction approach described in reference[2] along with the liner attenuation modeling approach described above has been applied to predict the nonlinear propagation of MPT tones in the inlet nacelle of a typical high bypass ratio engine during a static engine test. Two unsteady pressure transducers were installed inside the nacelle to measure dynamic pressure fluctuations on the casing. Transducers one and two are 1.25 and 1.74 tip chord upstream of the fan leading edge. In the prediction process, the pressure fluctuations at the fan leading edge have been reconstructed with the use of the 3-D CFD and superposition approach.[2] Nonlinear propagation and attenuation of the shock waves from the fan leading edge to the nacelle lip are computed using the 1-D propagation model. The result of the nonlinear propagation model at the transducer locations is compared to the static engine test data. Two cases of engine inlet nacelle

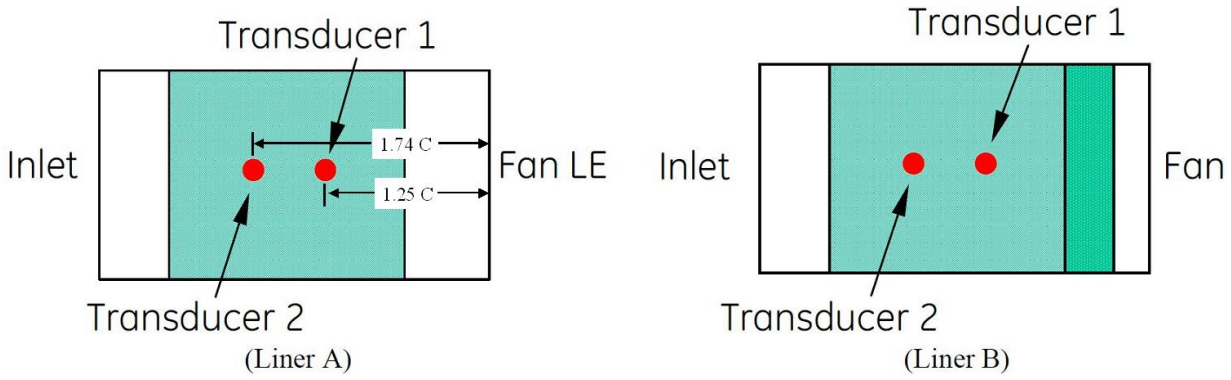

Figure 5. Two liner (shaded areas) configurations used in static engine test and predictions.

configurations were studied - 1) liner A; and 2) liner B. Sketches of axial locations of liner A and B are shown in Fig. 5. The results for the corresponding hard-wall configuration were presented in Ref.[2]

The measured and predicted sound pressure levels at the transducer 1 location in the casing are shown in Fig. 6, for the liner A and B configurations. In the calculations of nonlinear MPT propagation, the liner attenuation with the boundary layer effect included using the Myers-Chuang approach is compared with results assuming a uniform mean flow. The ratio of the boundary layer height to the casing radius used in the current calculation is 0.025. It can be seen clearly that the uniform flow assumption significantly over-predicts the liner attenuation, particularly for high order modes. In both liner configurations using the Myers-Chuang approach captures the liner attenuation effect very well.

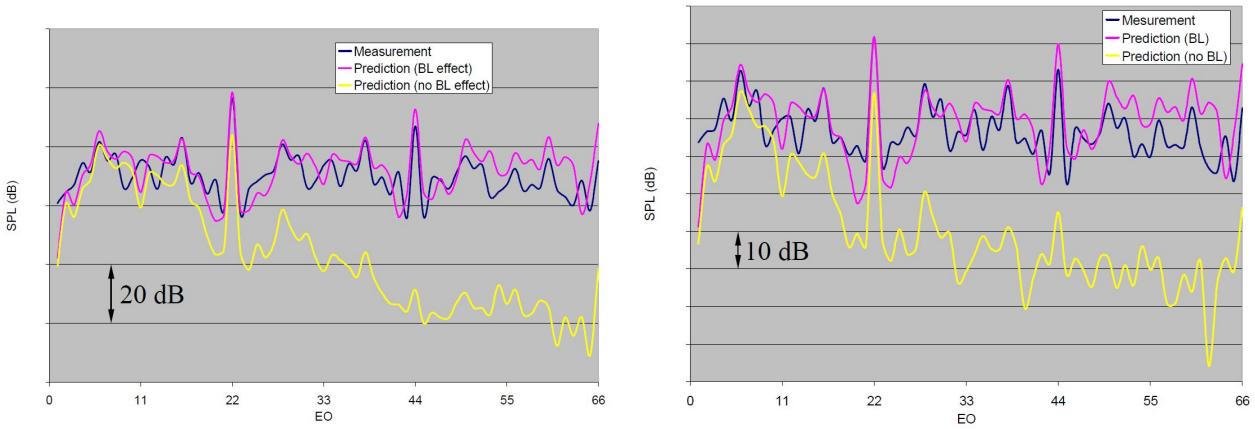

(a) Liner A (b) Liner B

Figure 6. Measured and predicted MPT spectrum at the transducer 1 location for the static engine test for - (a) liner A, and (b) liner B configurations.

To examine the liner attenuation effect more closely, measured SPL data at the transducer 2 location for the configuration A was subtracted from the measured SPL data at the same transducer for the hardwall configuration to obtain the net liner attenuation effect. Note the result is not the attenuation effect of the whole inlet liner, rather only of the section upto the transducer location. The result is plotted in Fig. 7 (a) along with predictions. Figure 7(b) shows similar results for the attenuation effect for configuration B. Except for modes around engine order 22, the predicted liner attenuation matches with measured data with reasonable agreement. The model over-predicts the attenuation around EO mode 22 by approximately 5 dB. Considering the very high over-prediction with zero BL thickness as shown in the figure, this is an improvement in prediction accuracy. However, the cause of the over-prediction at EO Mode 22 is not understood at the moment.

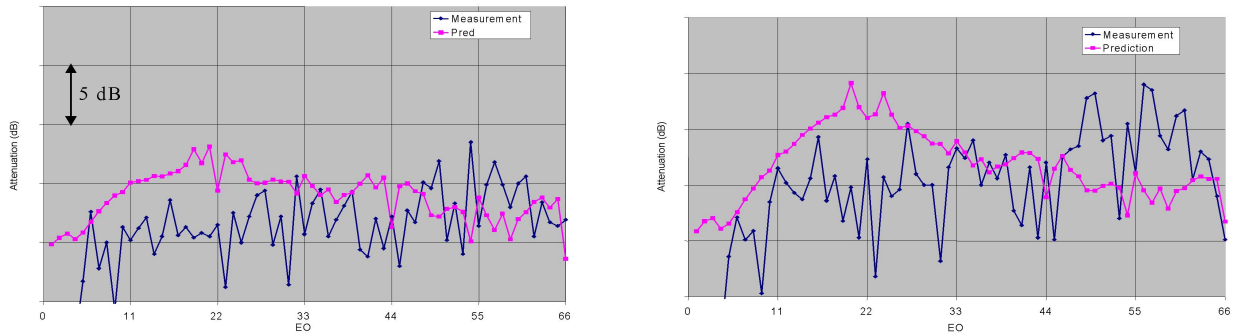

(a) Liner A

(b) Liner B

Figure 7. Measured and predicted liner attenuation effect for the static engine test case (a) Liner A; (b) Liner B.

V. Linear Propagation Results

The choice of the transition location between nonlinear and linear propagation is arbitrary at this point. In theory, the location should be determined by the appropriate amount of shock attenuation upstream of the fan blades so that nonlinear effects are minimized. In the case of a hardwall engine configuration, it is difficult to choose a location inside the engine nacelle that satisfies this criterion. Therefore, in Ref.[2] the engine inlet location was chosen that corresponds to the location of the bellmouth for the static engine test. For a lined engine configuration, the shock attenuates rapidly inside the nacelle, so the transition location is chosen such that the entire liner is being modeled by the nonlinear propagation code

Once MPT noise is propagated to the nacelle lip with the use of the 1-D nonlinear propagation model, the farfield radiation is computed with a linear acoustic propagation method.[2] For MPT noise, each harmonic tone of the engine shaft frequency corresponds to an acoustic mode in the nacelle. The modal circumferential order is the same as the harmonic order of the frequency, or the engine order (EO). ACTRAN/TM, a numerical code developed by Far Field Technologies, is used to simulate the linear acoustic mode propagation from the nacelle inlet to the far-field locations.

Modes of circumferential order 1 to 4 were cut-off because of the small associated frequency. So only far field results of mode 5 to 22 were obtained. Modes of order higher than 22 were not simulated because for the high computation time. A 2-D axi-symmetric approximation calculation using the nacelle profile from the 90% cut was carried out to obtain the SPLs at the microphone array locations for modes with circumferential order up to 66 or 3^{rd} BPF, since 2-D axi-symmetric calculation is much faster in terms of computational time. Two microphone arrays are used in the static engine test: one is an arc of microphones at a distance of 150 feet away from the engine center; the other group of microphones form a straight line located much closer to the engine, as shown in Fig. 8.

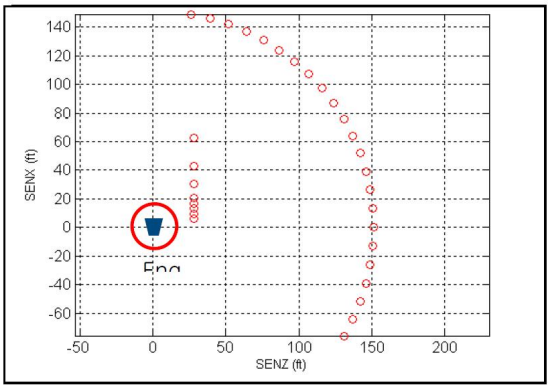

Figure 8. Microphone array locations in the static engine tests.

For brevity, the results of measured and predicted data for only configuration B are presented. Figures 12 and 10 show the directivity of SPLs at near field and far field microphone array locations for the mode of engine order 6 and 12, respectively. As with the complete hardwall configuration, both 3-D ACTRAN/TM model and 2-D axi-symmetric ACTRAN/TM model capture the measured data pretty well, with 2-D axi-symmetric approximation yielding lower SPLs at small angles at far field, due to its inability to model 3-D geometry and mean flow scattering effects in the linear propagation and radiation process. However, even the full 3-D approach under-predicts the measured SPLs at small angles, particularly at far field. This is because a 1-D nonlinear propagation was assumed from the fan leading edge to the nacelle lip, whereas in reality the 3-D nacelle geometry, meanflow, and liner will cause scattering of the acoustic energy into higher order radial modes.

Figure 10 shows the measured and predicted spectra at microphone locations (50^0 and 80^0) for configuration Liner B. The standard deviation between measured and predicted results for all modes is around 10 dB.

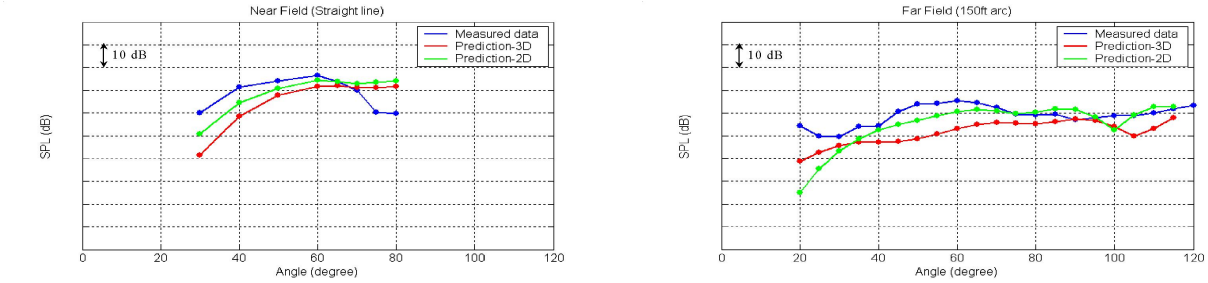

(a) Near-field (b) Far-field

Figure 9. Measured and predicted MPT SPL directivity at (a) near-field microphone array and (b) far-field microphone array for the static engine test case, EO= 6, for Liner B configuration.

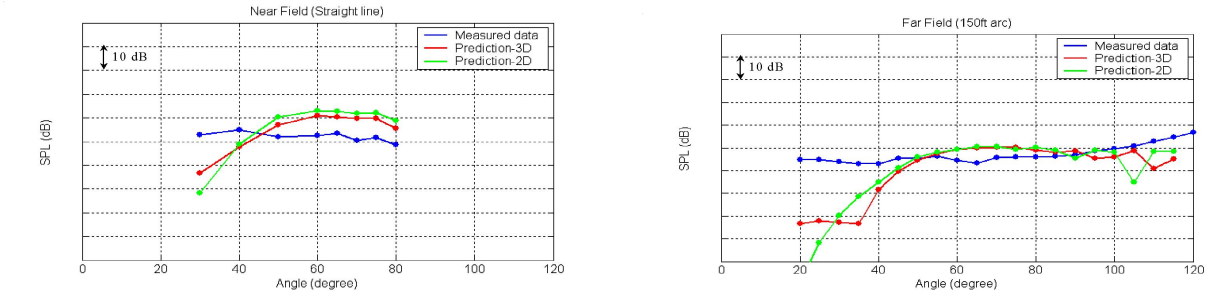

(a) Near-field (b) Far-field

Figure 10. Measured and predicted MPT SPL directivity at (a) near-field microphone array and (b) far-field microphone array for the static engine test case, EO= 12, for Liner B configuration.

The microphone data for the configurations with liners were subtracted from the microphone data for the complete hardwall configuration to obtain the net liner effect. Figure 13 (a) shows the attenuation effect for Liner A configuration. Figure 13 (b) shows the attenuation effect for Liner B configuration. The attenuation is calculated using averaged SPLs over all measurement angles, and the measured results are compared with predictions. Note that in the predictions the liner effect was modeled completely in the nonlinear propagation step of the process, as described before. Also, the nonlinear interaction term in the equation was removed to obtain just the linear liner attenuation results. Modes with engine order of $1-4$ are cut-off, so there were no data in measurements. The 1-D nonlinear code could not properly identify a mode being cut-on or cut-off, and gave a wrong prediction for these modes. For modes between 5 and 16, the model correctly predicted the measured liner attenuation. For modes above engine order 16, the model over-predicts the liner attenuation effect by 7.5 dB to 10 dB on an average.

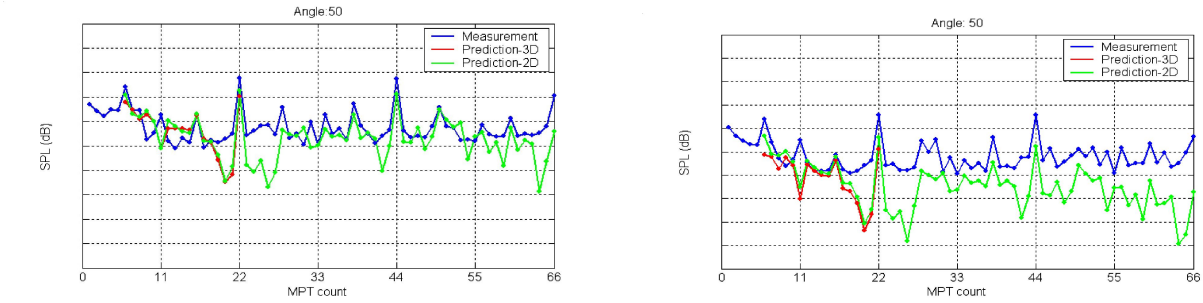

(a) Near-field (b) Far-field

Figure 11. Measured and predicted MPT SPL spectra at (a) near-field and (b) far-field at the 50^0 microphone for the static engine test case, for Liner B configuration.

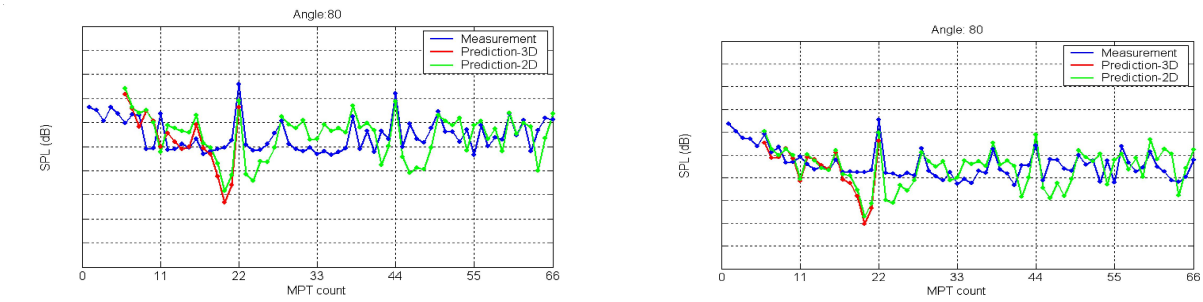

(a) Near-field (b) Far-field

Figure 12. Measured and predicted MPT SPL spectra at (a) near-field and (b) far-field at the 80^0 microphone for the static engine test case, for Liner B configuration.

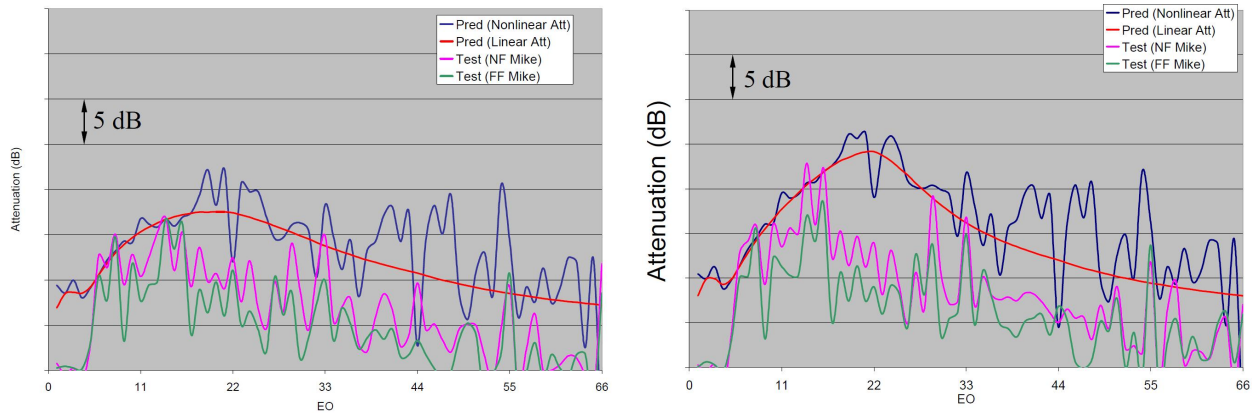

(a) Liner A (b) Liner B

Figure 13. Measured and predicted liner attenuation effect for the static engine test case: (a) Liner A, and (b) Liner B.

A. Trend Predictions

An investigation into the capability of the prediction process to predict the trend of MPT from one configuration to another was also carried out. To better compare the results, measured MPT SPL spectra from the angles 50^0 to 80^0 were averaged over locations to yield an averaged MPT spectrum. The power of each tone for all the tones from engine order 1 to 66 (up to the 3^{rd} BPF) were then summed to obtain an overall power, which was subsequently converted to an overall sound power level (OAPWL). Prediction results were post-processed the same way.

Figure 14 shows the trend of the overall sound power level of MPT from the hardwall nacelle configuration, to the Liner A configuration, and to Liner B configuration for the static engine test case. For all three configurations, the difference between measured and predicted OAPWL is within 4 dB. The attenuation effects of the liners are also predicted correctly.

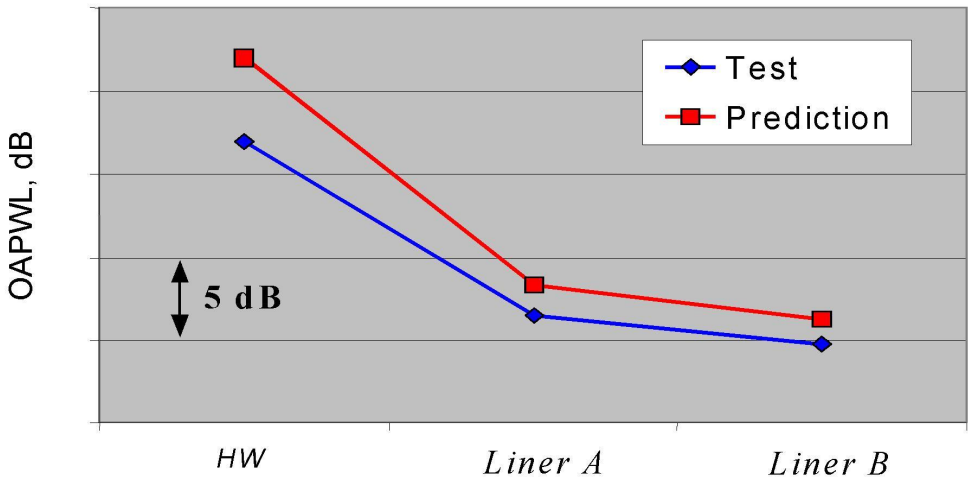

Figure 14. Measured and predicted MPT OAPWL for the static engine test case.

VI. Conclusions

A numerical procedure to predict the generation, in-duct propagation, and radiation of MPT noise for acoustically treated aero-engine inlets is developed. The procedure included four steps. First, Reynolds-Averaged Navier-Stokes (RANS) CFD simulations to generate the pressure field upstream of the as manufactured fan blades. Second, a linear superposition method was used to reconstruct the pressure field from CFD calculations using measured fan blade stagger angle distribution. This pressure distribution was then used as an input to a 1D non-linear propagation model to investigate the propagation of MPT from just upstream of the fan blades to the nacelle lip. In the last step in the prediction procedure, ACTRAN/TM was used for linear acoustic mode propagation and radiation from the nacelle lip to far-field locations. The entire analytical procedure was applied to a typical high bypass ratio engine during a static engine test. Different acoustic treatment configurations were tested. The predictions of MPT sound pressure levels were compared with measured data using transducers installed in the engine nacelles and far field microphones on the ground. In general, the predictions were found to be in good agreement with measured data. The SPL at small angles to the nacelle center axis was under predicted, as the prediction process ignored in-duct mode scattering.

VII. Acknowledgment

The authors would like to express their appreciations for the many useful discussions with Muni Majjigi, Richard Cedar, and Bryan Callender at GE Aviation, as well as John Premo and Cyrille Breard at the

Boeing Company.

References

[1]P. Gliebe, R. Mani, H. Shin, B. Mitchell, G. Ashford, S. Salamah, and S. Connel, "Aeroacoustic Prediction Codes," *NASA/CR–2000-210244*, 2000.

[2]F. Han, C. M. Shieh, A. Sharma, and U. Paliath, "Multiple Pure Tone Noise Prediction and Comparison with Static Engine Test Measurements," *13th AIAA/CEAS Aeroacoustics Conference, Rome, Italy*, 2007.

[3]A. McAclpine and M. J. Fisher, "On The Prediction of "Buzz-Saw" Noise in Aero-Engine Inlet Ducts," *Journal of Sound and Vibration*, Vol. 248, No. 1, 2003, pp. 123–149.

[4]A. McAclpine and M. J. Fisher, "On The Prediction of "Buzz-Saw" Noise in Acoustically Lined Aero-Engine Inlet Ducts," *Journal of Sound and Vibration*, Vol. 265, No. 1, 2003, pp. 175–200.

[5]*ACTRAN User's Manual*, 2005.

[6]W. Eversman, *Theoretical Models for Duct Acoustic Propagation and Radiation*, NASA Langley Research Center, Hampton, Virginia, 1991.

[7]W. Eversman, "Approximation for Thin Boundary Layers in the Sheared Flow Duct Transmission Problem," *The Journal of the Acoustical Society of America*, Vol. 53, No. 5, 1973, pp. 1346–1350.

[8]M. K. Myers and S. L. Chuang, "Uniform Asymptotic Approximations for Duct Acoustic Modes in a Thin Boundary Layer Flow," *AIAA Journal*, Vol. 22, No. 9, 1984, pp. 1234–1241.